Magnetic Resonance Imaging 55 (2019) 72–80

Contents lists available at ScienceDirect

Magnetic Resonance Imaging

journal homepage: www.elsevier.com/locate/mri

Original contribution

Mitral annular velocity measurement with cardiac magnetic resonance imaging using a novel annular tracking algorithm: Validation against echocardiography

Paaladinesh Thavendiranathan[a,b], Christoph Guetter[c], Juliana Serafim da Silveira[a], Xiaoguang Lu[c], Debbie Scandling[a], Hui Xue[d], Marie-Pierre Jolly[c], Subha V. Raman[a], Orlando P. Simonetti[a,*]

[a] The Ohio State University, Columbus, OH, USA
[b] Toronto General Hospital, Peter Munk Cardiac Center, University of Toronto, Toronto, ON, Canada
[c] Siemens Medical Solutions, Medical Imaging Technologies, Princeton, NJ, USA
[d] NHLBI, Bethesda, MD, USA

ARTICLE INFO

Keywords:
Diastolic function
Cardiovascular magnetic resonance
SSFP cine imaging
Echocardiography
Mitral annular velocity
Semi-automated annular tracking

ABSTRACT

Background: Doppler based mitral annular velocities are an integral part of echocardiographic left ventricular diastolic function assessment. Although these measurements can be obtained by phase contrast cardiac magnetic resonance imaging (PC-CMR), this approach has limitations. The aims of this study were to assess the accuracy and reproducibility of a high temporal resolution steady-state free precession (SSFP) cine acquisition coupled with semi-automated mitral annular tracking to measure tissue velocity, and compare to echocardiography as the reference method.

Methods: High temporal resolution (17 ms) 4-chamber cines were acquired in 25 volunteers using retrospective and prospective gating on a 3.0 T magnet. Mitral annular early (e′) and late (a′) tissue velocities were derived using a novel algorithm to semi-automatically detect the mitral valve insertion points and track its motion. Additionally, PC-CMR was used to measure mitral inflow early diastolic (E) velocity. Those measurements were also obtained using echocardiography based pulsed and tissue Doppler techniques, on the same day.

Results: Subjects were on average 34 ± 14 years-old (48% male). The lateral annulus e′ measurements had the best agreement with echocardiography with a concordance correlation coefficient (CCC) of 0.76 and 0.75 for prospectively and retrospectively gated cine CMR respectively. There was no significant difference in the lateral annular tissue velocities between echocardiography (13.8 ± 3.7 cm/s) and prospective (13.4 ± 3.7 cm/s) or retrospective (14.0 ± 3.7) acquisitions. Similarly, CMR measurement of E/e′ (a surrogate marker for LV filling pressures) using the lateral e′ velocity showed moderate agreement with echocardiography (CCC of 0.56 and 0.51 for prospective and retrospective acquisitions respectively) without a significant difference in ratios (5.3 ± 1.6 and 5.0 ± 1.3) compared to echocardiography (5.2 ± 1.4). Intra- and inter-observer reproducibility of the CMR-based annular velocity measurements was good.

Conclusion: Measurements of mitral annular tissue velocities can be obtained from SSFP 4-chamber cine images using a semi-automated annular tracking algorithm, and demonstrates moderate agreement with echocardiography. The semi-automated method can provide quantitative mitral annular velocity measurements directly from conventional cine images, thereby providing additional clinically relevant information. The accuracy of this method in patients with diastolic dysfunction remains to be determined.

Abbreviations: a′, late mitral annular tissue velocity; CCC, concordance correlation coefficient; CMR, cardiovascular magnetic resonance; E, PC-MRI derived early mitral inflow diastolic velocity; e′, early mitral annular tissue velocity; ICC, intraclass correlation coefficient; LV, left ventricle; PC-CMR, phase contrast cardiovascular magnetic resonance; SAR, specific absorption rate; SSFP, steady state free precession; TDI, tissue Doppler imaging; TE, echo time; TR, repetition time; TSENSE, time-adaptive sensitivity encoding; Venc, velocity encoding

* Corresponding author at: The Ohio State University, 460 W. 12th Ave, Room 320, Columbus, OH 43210, USA.
E-mail addresses: dinesh.thavendiranathan@uhn.ca (P. Thavendiranathan), christoph.guetter@gmail.com (C. Guetter), Juliana.Silveira@procardiaco.com.br (J.S. da Silveira), Xiaoguang.Lu@siemens.com (X. Lu), debbie.scandling@osumc.edu (D. Scandling), hui.xue@nih.gov (H. Xue), marie-pierre.jolly@siemens.com (M.-P. Jolly), Subha.raman@osumc.edu (S.V. Raman), Orlando.Simonetti@osumc.edu (O.P. Simonetti).

https://doi.org/10.1016/j.mri.2018.08.018
Received 6 July 2018; Accepted 27 August 2018

1. Background

Assessment of left ventricular diastolic dysfunction has diagnostic and prognostic value in patients with heart failure [1,2]. Although echocardiography is most commonly used for the non-invasive assessment of diastolic function [3,4], cardiac magnetic resonance (CMR) has an emerging role [3,5,6]. In addition to providing unique measures such as myocardial fibrosis [7,8], and edema [9–11], CMR can also provide the traditional parameters used to evaluate diastolic function without the limitations of acoustic windows that beset echocardiography [3–6,12–14]. Amongst the various diastolic parameters that can be measured by CMR, myocardial tissue velocity at the mitral annulus is especially important as it helps differentiate patients with normal versus stage 2 diastolic filling pattern, differentiate constrictive from restrictive cardiomyopathy, and allows the estimation of left ventricular filling pressures [4,12,14–16].

Studies using phase contrast CMR (PC-CMR) have been performed to measure myocardial tissue velocities at the mitral annulus, but only modest correlation with Doppler echocardiography has been shown [5,17]. Practically, this technique has several limitations including low temporal resolution [17], variability in the tissue velocity values depending on the location of measurement [5], susceptibility to background phase offset errors [17–19], and the need for significant manual interaction with the data [5]. Myocardial deformation parameters have been successfully extracted from steady state free precession (SSFP) cine images using CMR feature tracking algorithms [13,20,21], and myocardial tissue excursion at the mitral annulus has been measured using SSFP cine images by automatically detecting and tracking the mitral valve insertion points [22–24]. Such use of SSFP images to track myocardial displacement at the mitral valve insertions has the potential to overcome the previously described limitations associated with PC-CMR techniques. However, tissue velocities at the mitral annulus derived from CMR feature tracking have not been validated against tissue Doppler echocardiography. The objective of this study was to assess the accuracy and reproducibility of deriving tissue velocity at the mitral annulus from high temporal resolution SSFP cine images using Doppler echocardiography as the reference standard in healthy volunteers.

2. Methods

2.1. Study population

Healthy volunteers were recruited using local advertisements. All volunteers gave informed consent to undergo CMR and echocardiography exams within a few hours on the same day. Absence of cardiovascular disease or risk factors was confirmed by history at the time of enrollment. Volunteers with CMR contraindications were excluded. This study was approved by the hospital research ethics board.

2.2. CMR image acquisition and analysis

Retrospectively and prospectively gated breath-held cine SSFP images in the four-chamber view were acquired on a 3.0 Tesla scanner (Siemens, Tim Trio) using a 32-channel phased-array coil. Two ECG gating methods, prospective triggering and retrospective gating, were used and compared. Prospective triggering provides more precise timing of data acquisition with respect to the R wave, but the resulting images do not cover the entire cardiac cycle, missing late diastole. Retrospectively gated acquisition ensures that the entire cardiac cycle is covered, however temporal interpolation is employed in the reconstruction process. Images were planned with the medial and lateral mitral annulus included and the left ventricular outflow tract excluded. Common scan parameters used for both the prospectively triggered and retrospectively gated cine acquisitions were as follows: TR/TE = 2.5/1.1 ms, 108 × 192 matrix, and parallel imaging (GRAPPA) acceleration factor of 3. The flip angle was set to the maximum allowed by SAR limits and averaged 62° for retrospective and 47° for prospective triggering. An average field-of-view of 283 mm × 377 mm resulted in spatial resolution of 2.0 × 2.6 mm with an 8 mm slice thickness. For the prospectively gated acquisition, segmented k-space data (6 lines per segment) with true temporal resolution of 15.42 ms were acquired over a 12 heartbeat breath hold to reconstruct cardiac phases (frames) spanning approximately 1.5 heart beats; this modification to acquire data beyond one cardiac cycle was done to ensure that end diastole was imaged, which is not normally the case for prospectively triggered acquisitions. For the retrospectively gated acquisition, data were acquired with a true temporal resolution of 17 ms, and 60 frames were reconstructed regardless of heart rate; at an average RR interval of 937 ms, this resulted in an average reconstructed temporal resolution of 15.45 ms. A summary of acquisition parameters for prospective and retrospective cine imaging is presented on Table 1.

Table 1
Imaging parameters for prospective and retrospective cine SSFP imaging.

Imaging parameters	Prospective cine	Retrospective cine
Repetition time (TR)	2.5 ms	2.5 ms
Echo time (TE)	1.1 ms	1.1 ms
Flip angle	62°	47°
Slice thickness	8 mm	8 mm
Spatial resolution	2.0 × 2.6 mm	2.0 × 2.6 mm
True temporal resolution	15.42 ms	17 ms
Acceleration factor (GRAPPA)	3	3

In addition, a through-plane PC-CMR scan was run at the level of the mitral valve tips (set-up in diastole) parallel to the mitral annulus to measure early (E) diastolic mitral inflow velocity. Acquisition parameters were: TR/TE = 4.5/1.9 ms, 10 mm slice, 100 × 192 matrix, GRAPPA acceleration rate = 3, VENC = 150 cm/s, true temporal resolution 36 ms. A region of interest at the site of diastolic inflow was manually placed on one frame and propagated through all frames to measure the peak E velocity. The accuracy of propagation was verified on each frame and modified if necessary. All measurements were made by a reader blinded to the echocardiography data.

2.3. CMR annular velocity measurement

The mitral annular medial and lateral peak diastolic velocities were measured by semi-automated tracking of anatomical landmarks using both the retrospectively and prospectively gated datasets by a reader blinded to all other data. Time/velocity curves were generated and visually compared by the reader to the respective tracking results on the images (Fig. 1); manual adjustments to tracking points were made if errors in the automated tracking were visually detected. The tracking algorithm estimated the peak apex-to-base medial and lateral annular velocities using the acquired cine SSFP data in a semi-automated manner using the following steps: (i) the automatic detection of mitral valve insertion points [25], (ii) tracking of this position over the entire cardiac cycle using deformable registration [25], (iii) B-Spline interpolation of landmark positions for smooth time-velocity curves, and (iv) a manual correction by the user in cases of suboptimal automated tracking. Although components of the algorithm were previously described in detail elsewhere [22,25–27], the final complete algorithm demonstrated here is novel.

2.4. Landmark detection

The first step in the algorithm involved the detection of relevant anatomical landmarks. Landmark detection was used to automatically detect the mitral leaflet annular insertion points and the apex of the left ventricle. The algorithm employs a unified approach to anchoring components. This is a method of confirming that certain landmarks belong together as an anatomical group. These anchoring components

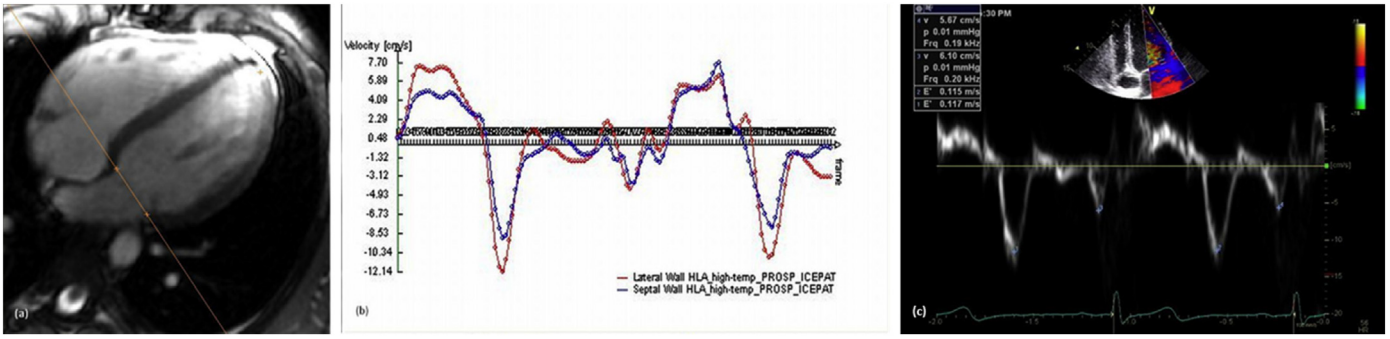

Fig. 1. Example of CMR and echocardiographic images and mitral annular velocity curves in one volunteer. The semi-automated annular tracking method is illustrated in panel A with the mitral annular lateral and medial velocities for 1.5 cardiac cycles in panel B. The lateral annular tissue velocities (Panel C) by echocardiography are shown. Mean lateral e′ velocities are 11.6 cm/s (echo) and 11.9 cm/s (CMR prospectively triggered), while the a′ velocities were 5.8 cm/s (echo) and 4.9 cm/s (CMR). (For interpretation of the references to colour in this figure, the reader is referred to the web version of this article.)

are then converted into parameterized bounding box representations that fit into an object detection framework. Such representation embeds not only individual anchoring components but also their context that contains rich information to distinguish the anchoring components from its background and other anatomical structures. We applied a learning-based method to train the detectors using expert, manual annotations in order to handle complex appearance and heterogeneous characteristics of anatomical features in medical images, as the complex prior knowledge is implicitly encoded. Learning based object detection approaches have been demonstrated successfully in other medical imaging applications [27,28].

The fully automated landmark detection approach can be flexibly applied to a wide range of anatomical structures. For example, our framework has been applied to detect the LV basal mitral valve plane and LV apex in long-axis images, as shown in Fig. 1, as well as RV insertion points to the LV, and RV lateral annulus (a point where the RV outer boundary changes directions significantly within the image) in short-axis images. We validated our approach on 8304 long-axis images, containing 4-, 3-, and 2-chamber views, using a 4-fold cross-validation scheme [26]. In each of these images, the base plane (two annulus anchors) and the apex of the LV were manually annotated by experts and used as the reference standard for evaluation. The overall performance of the mitral annulus anchor points on all the images was 5.1 ± 6.8 mm (mean ± SD) with a median of 3.7 mm proving to be robust and accurate for the purposes of tracking the mitral valve annulus velocities. However, post detection the frame to frame registration accuracy is sub-pixel, i.e. < 2 mm on this data [25].

2.5. Tracking in time series data using deformable registration

In order to track the detected mitral annulus points, we employ a symmetric and inverse-consistent deformable registration technique [25] to register all images of the given time series. This allows us to automatically propagate the annulus anchor locations throughout the time series following the tissue motion. Deformable image registration between two images is performed as follows. Consider two images described by the square-integrable functions $\boldsymbol{f_1 : \mathbb{R}^n \mapsto \mathbb{R}}$ **and** $\boldsymbol{f_2 : \mathbb{R}^n \mapsto \mathbb{R}}$. Deformable image registration searches for a function $\boldsymbol{\Phi_{12} : \Omega \to \Omega}$ that transforms each location $\boldsymbol{x}$ **in** $\boldsymbol{\Omega}$ ($\boldsymbol{\Omega}$ is a bounded region of $\boldsymbol{\mathbb{R}^n, n = 2,3}$) using a displacement field $\boldsymbol{u : \Omega \to \mathbb{R}^n}$ such that both images are accurately aligned: $\boldsymbol{\Phi_{12}(x) = x + u(x)}$. This function is searched in a set of admissible functions such that it minimizes an energy functional $\mathcal{J}$, and the minimizing function $\widehat{\boldsymbol{\Phi}}$ presents the solution of the deformable registration problem:

$$\widehat{\Phi} = \arg\min \mathscr{J}(f_1, f_2; \Phi_{12}) \tag{1}$$

where $\mathscr{J}$ depends on the two images f_1, f_2 and Φ_{12} describing the transformation from f_1 to f_2. The deforming function Φ_{12} can be retrieved by descending the gradient of $\mathscr{J}$ using an iterative scheme of composing incremental updates of the deformation:

$$\Phi_{12,k+1} = \Phi_{12,k} \circ (\mathrm{id} + \tau \cdot \nabla_u \mathscr{J} \star G_\sigma) \tag{2}$$

with τ controlling the step size along the gradient, and G_σ denoting a Gaussian filter. Step size parameter τ describes a trade-off between speed and accuracy.

We then use the theory of multi-objective optimization to leverage an interleaved optimization scheme subject to constraints of symmetry and inverse-consistency of the estimated image alignment. In this optimization scheme the gradient of a symmetric energy functional is descended by alternating the registration direction after each iteration. At the same time, inverse consistency is enforced through updating the inverse direction. The numerical implementation of this scheme can be done efficiently and the resulting algorithm requires little extra time per iteration when compared to a highly optimized, one-directional method. The proposed method has been found to provide accurate image registration while requiring significantly less time to be computed than state-of-the-art symmetric registration methods.

Annular tracking was performed using the local cross-correlation (LCC) because it has been proven to be a robust and accurate similarity measure for mono-modal image registration. The LCC for 2d images, i.e. $f \in \mathbb{R}^2$,is defined as:

$$\mathscr{J}(f_1, f_2, \Phi_{12}) = -\sum_{i,j}^{N_{nb}} \frac{\sum_{nb}(f_1(i,j) - \overline{f_1})(f_2 \circ \Phi_{12}(i,j) - \overline{f_2})}{\sqrt{\sum_{nb}(f_1(i,j) - \overline{f_1})^2 \sum_{nb}(f_2 \circ \Phi_{12}(i,j) - \overline{f_2})^2}} \tag{3}$$

where $\overline{f_1}$ and $\overline{f_2}$ are the mean values of the neighborhood *nb* around location $(i,j) \in \mathbb{R}^2$ in both images, and N_{nb} determines the number of elements in that neighborhood. The symmetric formulation of LCC can be written as:

$$\mathscr{J}(f_1, f_2, \Phi) = \mathscr{J}(f_1, f_2, \Phi_{12}) + \mathscr{J}(f_2, f_1, \Phi_{21}) \tag{4}$$

, with

$$\mathscr{J}(f_2, f_1, \Phi_{21}) = -\sum_{i,j}^{N_{nb}} \frac{\sum_{nb}(f_1 \circ \Phi_{21}(i,j) - \overline{f_1})(f_2(i,j) - \overline{f_2})}{\sqrt{\sum_{nb}(f_1 \circ \Phi_{21}(i,j) - \overline{f_1})^2 \sum_{nb}(f_2 \circ \Phi_{12}(i,j) - \overline{f_2})^2}} \tag{5}$$

Using an interleaved optimization scheme, we are able to find a deformation field Φ that fulfills the symmetric constraint of Eq. (4) (see reference [25] for details on the optimization). This deformation field presents an accurate and consistent solution between two images.

In order to track the changing location of an anatomical feature such as the mitral annulus throughout a cardiac cycle, we register the available cine time series images using the algorithm described [25]. To achieve this registration, we pick a keyframe, e.g., the first frame in the series that typically represents the end-diastolic phase (ED), to which

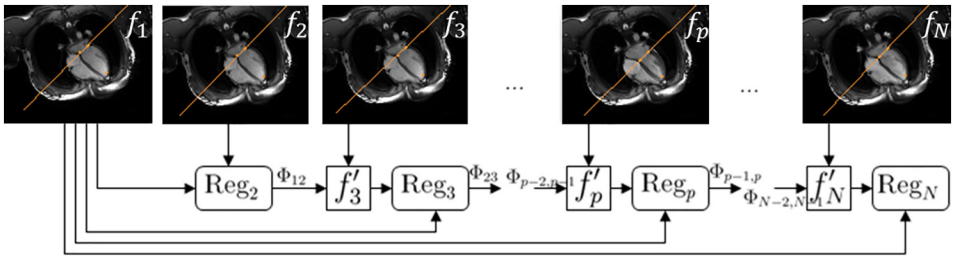

Fig. 2. An illustration of the consecutive deformable registration scheme for registering cardiac MR time series data. Images f_1, …, f_N are registered pair-wise with its temporal neighbor resulting in registration Reg_2, …, Reg_N whose outcomes are deformation fields Phi_ij for images f_i and f_j. Deformation field Phi_ij will be used to initialize the registration procedure Reg_j + 1 through warping image f_j + 1 yielding image f′_j + 1.

all other phases are connected by the deformation field. The registration, however, is performed on consecutive images or phases, and the consecutive deformation fields are then concatenated with all previous phases in order to link the deformation field to the keyframe. Fig. 2 illustrates the consecutive registration scheme on a series of mid-ventricular cardiac MRI images.

The automatically detected and tracked mitral annulus and apex landmarks are further smoothed using B-Spline interpolation in order to suppress variations in spatial location over time that are due to image noise. An example time/velocity curve that is produced by the automated tracking algorithm is shown in Fig. 1b.

A further optimization of the consecutive registration scheme can be employed when the image series represents a complete cardiac cycle, as it typically does in retrospectively gated cine acquisitions. In this case, the first and last frame of the series can be considered to be adjacent in time, and the registration algorithm can be started in two directions simultaneously, i.e., for frames 0, 1, …, N/2-1, and for frames 0, N-1, N-2, …, N/2. While both series share keyframe 0, they are otherwise treated as independent of each other. There are two advantages in this optimization: (i) when using a multi-core computer system, the registration of the two series can be performed in parallel, and (ii) potential error accumulation propagates only through half the series and can be minimized by registering the end points of each series; i.e., images *N/2–1* and *N/2* where *N* is the number of images or phases in the time series.

The automated mechanism of tracking mitral valve insertion points on cine MR images (Fig. 1a) throughout the cardiac cycle was combined with a user interface designed to support manual correction of the automated results in a standalone program running on an independent computer workstation. DICOM images were exported from the MRI system and read directly into this program for analysis.

2.6. Deriving peak velocities

The automatically generated velocities for each temporal frame in the cine sequence were plotted against time and the medial and lateral annular early (e′) and late (a′) diastolic peak tissue velocities were identified as the highest velocity at the time of early relaxation and atrial contraction, respectively. Fig. 1a shows the detection of the mitral valve insertion points at the medial and lateral annulus, and Fig. 1b depicts the velocity/time curve as a result of the tracking for medial (blue) and lateral (red) annular points. Fig. 3 shows the tracking results for three different data sets through selected images of the acquired time series. The figure shows how the algorithm is capable of dealing with varying image qualities and information to achieve visually accurate tracking performance.

In the same cohort of 25 subjects, mitral inflow velocities and tissue velocities were extracted from PC-CMR images and cine SSFP images, as well as Tissue Doppler Imaging (TDI) echocardiography. The data were acquired on the same day for each subject and all image processing and data analysis was performed retrospectively. Mitral inflow velocities E and A, and e′, a′ velocities for medial and lateral wall motion were measured in order to compare lateral, medial, and combined e′, a′ and E/e′ between the two modalities.

2.7. Echocardiography acquisition and analysis – reference standard

All echocardiography studies were performed by an experienced sonographer using a GE system (Vivid 7) with a 4 MHz 2-D transducer (GE Healthcare, Milwaukee, Wisconsin). Echocardiography data were acquired on the same day as the CMR study for each subject. Mitral inflow velocities were measured from the apical 4-chamber view using a 2–5 mm pulsed wave Doppler sample volume placed at the tip of the mitral valves as per guidelines [4]. Similarly, from apical views the mitral annular medial and lateral tissue velocities were measured using tissue Doppler imaging and a 2 mm pulsed wave Doppler sample volume. Acquisition settings were optimized to obtain the highest temporal resolution (> 70 Hz) and minimization of pulsed wave spectral broadening. All mitral inflow and tissue Doppler velocities were measured and averaged across 3 consecutive heart beats. All measurements were performed by an experienced dedicated research echocardiography technologist in a core lab setting blinded to all CMR data.

2.8. Reproducibility

In 10 subjects, the inter-observer variability of the algorithm for measurement of medial and lateral annular velocities was assessed by two readers blinded to each other's results. The intra-observer variability was also assessed by one reader by re-measuring the velocities in 10 patients 4 months later, blinded to their previous measurements.

2.9. Statistical analysis

Continuous data with normal distribution are expressed as mean ± standard deviation, and non-normally distributed data as median and interquartile range. All annular and mitral inflow velocity measurements were normally distributed as determined using the Kolmogorov-Smirnov test and visual inspection of the data using normal plots. The presence of outliers was determined using the Outlier Labeling Rule [29]. Paired *t*-test was used to test difference between measurements. Since 3 comparisons were made for some analyses, a $p < 0.0167$ was considered statistically significant. Agreement between methods was examined using Bland-Altman analysis and Lin's Concordance Correlation Coefficient (CCC) and intra-class correlation (ICC). Inter- and intra-observer variability was assessed using ICC and coefficient of variation (COV). All statistical analysis was done using MedCalc (11.4.2.0, Mariakerke, Belgium) and SPSS (19.0.0, IBM Corporation, Chicago, IL).

3. Results

3.1. Volunteer demographics and feasibility

A total of 25 volunteers (12 male, 13 female) were included with a mean ± standard deviation (mean ± SD) age of 34 ± 14 years, range 18–65 years. Measurement of e′ and a′ velocities using both prospectively and retrospectively gated cine CMR images and the automated algorithm was feasible in all subjects for both the medial and lateral annulus. In all cases at least one manual correction step was performed on the tracked landmarks to correct for algorithm

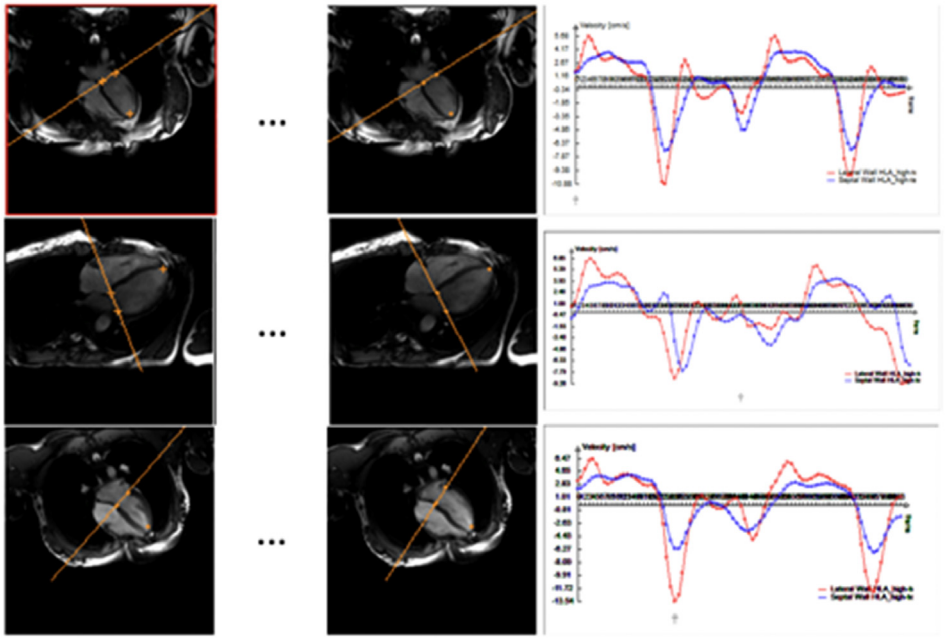

Fig. 3. Examples of CMR long-axis images and velocity curves in three different volunteers showing the annulus velocities that result from semi-automatic tracking of mitral valve insertion points.

instabilities due to image noise, acquisition length (e.g. > 1 cardiac cycle in prospectively triggered acquisitions), and signal variations caused by blood-flow that "distracted" the deformable registration algorithm. The approximate time necessary to automatically track the annulus and obtain velocities was < 1 min, however, if manual adjustment was necessary processing time can increase by up to 10 min. The measurement of mitral inflow E velocity by CMR and echocardiography and annular velocities by echocardiography was feasible in all volunteers.

3.2. Annular velocity measurements

The mean ± SD measurements of mitral annular medial and lateral velocities for the prospective and retrospective acquisitions are summarized in Table 2. There was no statistically significant difference in medial and lateral e′ velocities obtained using either prospectively or retrospectively gated cine CMR data in comparison to echocardiography (Table 2). However, the a′ velocities were underestimated by both CMR techniques in comparison to echocardiography for both the medial and lateral annuli. The CCC/ICCs for comparisons of prospectively gated CMR acquisition with echocardiography for the medial and lateral e′ velocities were 0.65 (95% CI 0.38–0.82)/0.65 (95% CI 0.36–0.83) and 0.76 (95% CI 0.54–0.89)/0.77 (95% CI 0.55–0.89), respectively, while for a′ velocities they were 0.27 (95% CI 0.09–0.45)/0.03 (95% CI −0.36–0.41) and 0.51 (95%: 0.25–0.71)/0.46 (95% CI: 0.10–0.72). For comparison, the CCC/ICCs of retrospectively gated CMR acquisition with echocardiography, were 0.60 (95% CI 0.28–0.80)/0.61 (95% CI: 0.30–0.81) and 0.75 (95% CI 0.51–0.88)/0.75 (95% CI: 0.53–0.88) for medial and lateral e′ velocities, and 0.31 (95% CI 0.08–0.50)/0.14 (95% CI: −0.25–0.50) and 0.39 (95%: 0.05–0.64)/0.36 (95% CI −0.03–0.65) for medial and lateral a′ velocities. When prospective and retrospective gated acquisitions were compared to each other there was no statistically significant difference between the lateral velocity measurements, but there was a significant difference in the medial annular velocities. Bland Altman comparisons for the various annular velocities are presented in Fig. 4. There was minimal systematic bias for the medial and lateral annular e′ velocities, however, the a′ velocities were underestimated by CMR. The relationship between age and annular velocities are illustrated in Fig. 5 for the retrospectively gated CMR acquisition. An identical trend was seen for prospectively gated cine CMR (data not shown).

Table 2
Comparison of annular velocities between echocardiography and semi-automated annular tracking using prospectively and retrospectively gated CMR data.

	CMR prospectively gated	CMR retrospectively gated	Echocardiography
Medial annulus e′ (cm/s)	9.3 ± 3.1†	10.7 ± 3.0	10.5 ± 2.9
Medial annulus a′ (cm/s)	4.3 ± 1.9*	4.5 ± 2.6*	7.2 ± 2.0
Lateral annulus e′ (cm/s)	13.4 ± 3.7	14.0 ± 3.7	13.8 ± 3.7
Lateral annulus a′ (cm/s)	5.3 ± 2.3*	5.7 ± 2.6*	7.1 ± 2.5
E/e′ ratio medial	7.9 ± 2.7†	6.6 ± 1.7	6.9 ± 2.1
E/e′ ratio lateral	5.3 ± 1.6	5.0 ± 1.3	5.2 ± 1.4
Mitral inflow E velocity (cm/s)	68 ± 18		67 ± 15

* $p < 0.0167$ in comparison to echocardiography, †$p < 0.05$ between the two CMR methods.

3.3. Mitral inflow E velocity and filling pressure estimation

The mean ± SD mitral inflow E velocities are summarized in Table 2. There was no significant difference in this measurement between PC-CMR and echocardiography ($p = 0.66$). The CCC/ICC for comparison of mitral inflow E velocities between echocardiography and CMR was 0.73 (95% CI 0.48–0.87)/0.73 (95% CI: 0.48–0.87).

The E/e′ ratio for medial and lateral annulus for the prospective and retrospective acquisitions and echocardiography are summarized in Table 2. There were no significant differences in these measurements between the two techniques with respective p values ranging from 0.08–0.64. There were no significant differences between the two CMR techniques for E/e′ ratio for the lateral annulus, however E/e′ calculated using the medial annulus velocity was significantly higher with

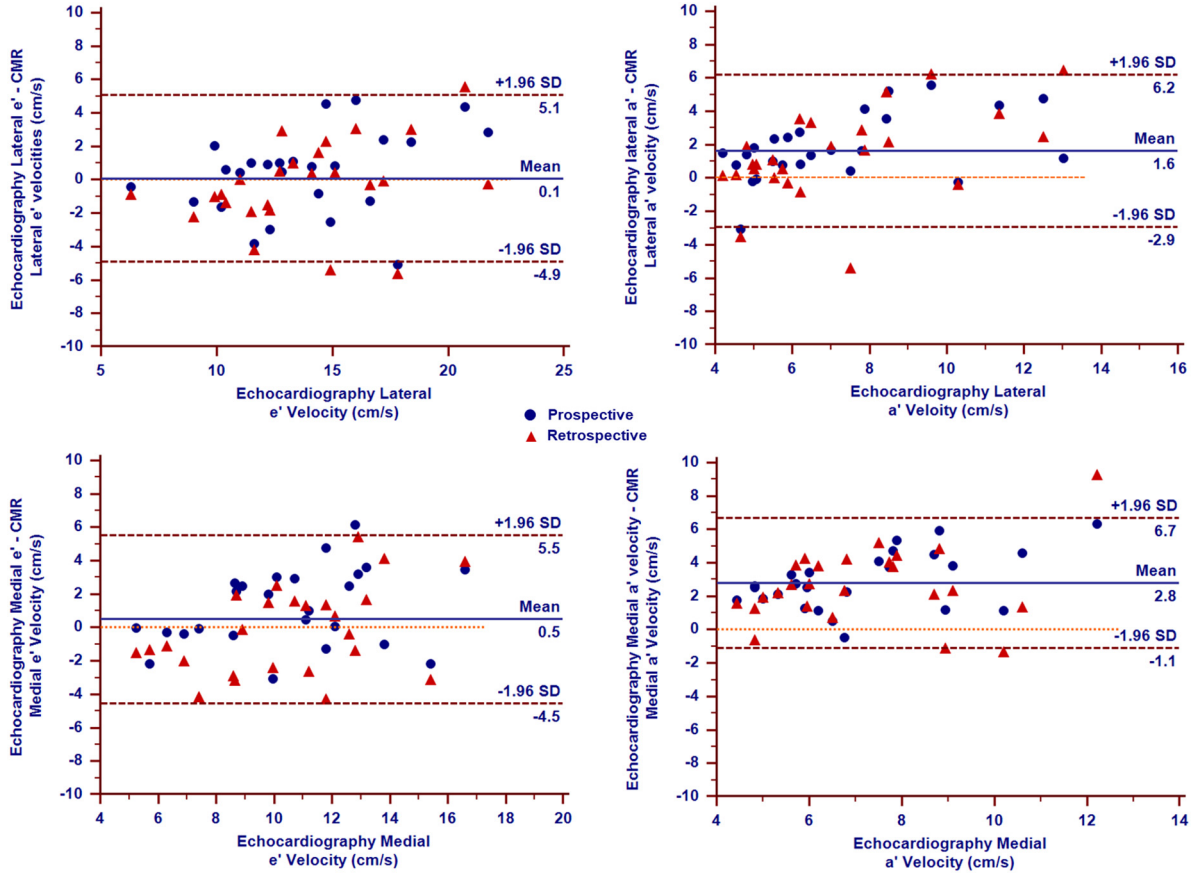

Fig. 4. Bland-Altman comparison of CMR and echocardiography measurements of annular velocities. There was minimal bias between the methods for comparison of e′ velocities, however there was a larger bias for the a′ velocities.

the prospectively triggered acquisition. The CCC/ICCs for the E/e′ ratio between echocardiography and prospectively triggered cine CMR for the medial and lateral annulus were 0.33 (95% CI −0.02–0.61)/0.32 (95% CI: −0.07–0.63) and 0.56 (95% CI: 0.23–0.78)/0.57 (95% CI: 0.24–0.79), respectively; the CCC/ICCs for the same comparisons between echocardiography and retrospectively gated cine CMR were 0.19 (95% CI −0.20–0.53)/0.20 (95% CI: −0.19–0.55) and 0.51 (95% CI 0.15–0.75)/0.52 (95% CI:0.17–0.75), respectively.

3.4. Observer variability

Mitral medial and lateral early annular (e′) velocities presented better inter-observer agreement for both prospectively and retrospectively gated CMR acquisitions (ICC ≥ 0.80, COV 4.7–11.4%), when compared with late (a′) diastolic velocities (ICC ≥ 0.38, COV 22.8–23.8%), as summarized in Table 3. The intra-observer agreement of early (e′) diastolic velocities was again significantly higher (ICC ≥ 0.86, COV 4.8–13.4%) than late (a′) diastolic velocities (ICC ≥ 0.44, COV 8.7–17.8%).

4. Discussion

This study illustrates the use of a semi-automated method to measure mitral annular velocities using high temporal resolution CMR 4-

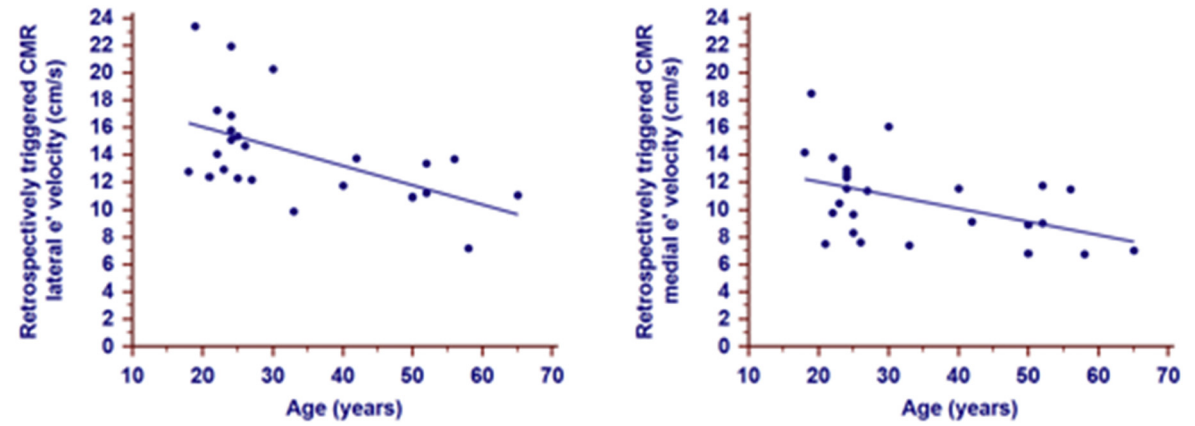

Fig. 5. Relationship between age and annular velocities for the retrospectively triggered CMR acquisition. The correlation for the lateral e′ velocity with age was −0.55, with medial e′ it was −0.47.

Table 3
Inter- and intraobserver agreement.

	Interobserver				Intraobserver			
	Prospective		Retrospective		Prospective		Retrospective	
	ICC (95% CI)	COV (%)	ICC (95% CI)	COV	ICC (95% CI)	COV	ICC (95% CI)	COV
Lateral e′	0.96 (0.84–0.99)	4.7%	0.86 (0.52–0.96)	10.4%	0.97 (0.88–0.99)	4.0%	0.98 (0.90–0.99)	4.8%
Lateral a′	0.75 (0.31–0.93)	23.8%	0.67 (0.07–0.90)	15.0%	0.86 (0.56–0.96)	12.7%	0.95 (0.72–0.99)	8.7%
Medial e′	0.80 (0.33–0.95)	11.1%	0.88 (0.60–0.97)	10.8%	0.92 (0.73–0.98)	6.6%	0.86 (0.53–0.96)	13.4%
Medial a′	0.39 (−0.15–0.79)	22.8%	0.38 (−0.36–0.80)	16.8%	0.71 (0.21–0.92)	13.2%	0.44 (−0.24–0.83)	17.8%

chamber cine images. The measured annular velocities showed moderate agreement with those obtained by Doppler echocardiography, which was used as the reference standard. The velocities were also in keeping with previous findings that in normal subjects the lateral annular velocities are higher than the medial, and that annular velocities decrease with age [30]. Furthermore, there was moderate agreement between the CMR measurement of E/e′ and echocardiography specifically in the lateral annulus. The annular measurements had good inter- and intra-observer reproducibility specifically for the measurement of early diastolic velocities.

4.1. Current methods and limitations

Heart failure is one of the leading forms of heart disease in the United States [31] with up to 40–50% of the patients having normal systolic function with diastolic dysfunction being the primary cause of the symptoms [1,32]. Furthermore, diastolic function assessment has important prognostic value both in patients with systolic and diastolic heart failure [33,34]. Although echocardiography has been the predominant method used for the non-invasive assessment of diastolic function and LV filling pressures, CMR has an important role as an adjunctive test when TTE data cannot be obtained due to poor acoustic windows, or when CMR is prescribed for the assessment of LV systolic function or myocardial viability. A comprehensive assessment of diastolic function is feasible by CMR using PC-CMR sequences to measure mitral inflow and annular velocities and pulmonary vein flow velocities [35]. However, PC-CMR has limitations when used for tissue velocity measurements due to the strong dependence on the site of measurement [5], annular plane through-plane motion, and phase offset errors. Furthermore, studies based on PC-CMR acquisitions have required manual positioning of the region of interest on each phase of the cardiac cycle, making this measurement time consuming and subjective. As a consequence, the use of CMR in clinical evaluation of diastolic function has remained limited.

4.2. Novel method for measuring annular velocities

The use of high temporal resolution cine CMR to measure mitral annular velocities by semi-automated annular detection and tracking is a novel method for the determination of annular velocities. The level of automation improves the workflow and inter-observer variability of the obtained measurements. The ability to visualize the translation of the annulus from the cine images provides an opportunity to verify the adequacy of the tracking algorithm and make adjustments as needed. With the completely automated algorithm, the annular detection, tracking, and velocity measurements are obtained in < 1 min on standard PC hardware. When manual adjustments to annular tracking are made, this can take up to 10 min. Furthermore, the high temporal resolution that is obtainable using cine CMR compared to traditional PC-CMR sequences ensures that the peak tissue velocities are more likely to be accurately captured. Also, concerns about phase offset errors which continue to plague PC-CMR acquisitions are avoided with this method [18,19].

The agreement between this new method and Doppler echocardiography for annular velocity measurements is consistent with the moderate correlation demonstrated previously by Paelinck et al. using PC-CMR acquisition in comparison to echocardiography (Pearson's $r = 0.49$) [5]. This correlation of 0.49 in their study was the best value amongst multiple measurements obtained at several locations around the mitral annulus. Other studies have also illustrated only modest agreement with echocardiography [17]. This may reflect the fundamental differences in the measurement of tissue velocities by the two modalities, and the angle dependence of the velocity measurements with echocardiography. Also, the agreement in E/e′ ratio in this study is similar to Paelinck et al.'s results where the r values were 0.59 and 0.38 for the medial and lateral annular measurements respectively. They did, however, report a higher correlation for the best annular measurement obtained from the posterior inter-ventricular septum; a location which was not available for measurement in our 4-chamber images. Other studies [35,36] have reported higher correlations for the annular velocities and E/e′ ratio likely reflecting the inclusion of normal and abnormal subjects in the same analysis (hence increasing the distribution of the data on the x-axis), and the use of long axis PC-CMR acquisitions with in-plane velocity encoding. The latter is also subject to limitations by the need to make adjustments to the site of tracking through each phase of the cardiac cycle due to translation of the mitral annulus.

There was relatively poor agreement in the a′ velocities obtained with CMR versus echocardiography in this study. This may illustrate the need for even higher temporal resolution than that obtained with the cine sequences used in this study. However, previous work with this semi-automated algorithm has illustrated that the amount of noise in the measurement increases as the temporal resolution increases [22]. Despite this, the measure of a′ velocity has limited clinical utility and has not been recommended in guidelines for the assessment of diastolic class or filling pressures [4].

This study also uniquely demonstrates the use of both retrospectively gated and prospectively triggered cine acquisitions with the semi-automated algorithm. The agreement with echocardiography was similar with either method, however the absolute velocity measurements were slightly higher with the retrospective compared to the prospectively triggered scans despite the fact that temporal interpolation is inherently used in the reconstruction. Furthermore, images spanning the entire cardiac cycle including late diastole are more efficiently acquired with retrospective acquisitions.

4.3. Other novel methods to measure diastolic function

There has also been a growing interest in the use of myocardial strain imaging to measure LV diastolic function and left atrial function [37]. Myocardial tagging or feature tracking algorithms can be used on cine SSFP images to measure LV diastolic strain. Also the feature tracking algorithms allow measurement of left atrial strain and strain-rate providing an assessment of left atrial reservoir, conduit, and booster pump function [38]. Left atrial function changes appear to be associated with diastolic dysfunction and correlate with exercise tolerance [39]. The temporal changes in LA function in relationship to

diastolic strain parameters remains to be determined. It is likely that mitral inflow and annular measurements as proposed by our algorithm and LV and LA strain analysis will play complementary roles in the assessment of diastolic function.

4.4. Limitations

The study had a small sample size and investigated only healthy volunteers; however, our sample size was not significantly different from previous studies on this topic [5]. The focus on healthy volunteers is a reflection of the fact that this is the first study assessing the accuracy and reproducibility of this method in the clinical setting with a reference standard. Future studies should focus on differentiating grades of diastolic dysfunction in patients and correlation of filling pressures with invasive angiography. The level of manual adjustment required with the tracking algorithm was probably mostly due to the artifacts caused by field inhomogeneity and blood flow that are commonly encountered with SSFP cine imaging at 3.0 T. The artificial image features created by these artifacts sometimes caused the tracking algorithm to lose its identification of the annulus. Therefore at present the potential need for manual adjustment and the associated time requirement (~10 min) may impact clinical application. However, the level of automation and tracking performance will be improved in the future, especially at lower field strength where these artifacts are less significant. Although the comparison between CMR and echocardiography using CCC and ICC only showed modest correlation, the level of agreement was consistent with previous studies [5,17] and likely reflects the fundamentally different techniques used to measure the annular velocities and the inclusion of healthy volunteers only. The automated tracking algorithm has some intrinsic limitations including the inability to track through plane motion and the application to only 2-dimensional data. Regardless, similar approaches with echocardiography to measure diastolic function have been shown to have tremendous prognostic value. Finally, this is a novel algorithm that would require clinical validation and experience before clinical application, however, the semi-automated methodology makes it adaptable to clinical practice.

4.5. Conclusions

This study illustrates the use of high temporal resolution cine CMR acquisition coupled with an efficient semi-automated mitral annular tracking method to measure mitral annular velocities. These measurements can be used in conjunction with other CMR measurements of diastolic function to determine diastolic class. Specifically, the e′ velocity can be combined with the early mitral inflow E velocity to estimate the E/e′ ratio as a marker of LV filling pressure. With this new algorithm an agreement with echocardiographic measurement was best achieved using the lateral annular velocities. Although there was only moderate agreement in the annular velocity and E/e′ ratio between CMR and echocardiography, the level of agreement was consistent with previous studies using PC-CMR, and this semi-automated method should have workflow advantages that will support the use of CMR for the assessment of diastolic function. Ultimately, the accuracy of this method in patients with various degrees of diastolic dysfunction must be investigated.

Competing interests

Christoph Guetter, Xioaguang Lu, Hui Xue, and Marie-Pierre Jolly were employed by Siemens Corporation at the time this study was performed. Xiaoguang Lu and Marie-Pierre Jolly are currently employed by Siemens Medical Solutions.

OPS and SVR receive research support from Siemens.

None of the authors have non-financial conflicts of interest.

Funding

Research reported in this publication was supported by the National Institutes of Health under award number **NHLBI R01 HL102450**. The content is solely the responsibility of the authors and does not necessarily represent the official views of the National Institutes of Health. The Robert F. Wolfe and Edgar T. Wolfe Foundation also provided support for this research. Dr. Thavendiranathan is supported by the Canadian Institutes of Health Research New Investigator Award (FRN 147814).

References

[1] Bhatia RS, Tu JV, Lee DS, et al. Outcome of heart failure with preserved ejection fraction in a population-based study. N Engl J Med 2006;355(3):260–9.
[2] Maeder MT, Kaye DM. Heart failure with normal left ventricular ejection fraction. J Am Coll Cardiol 2009;53(11):905–18.
[3] Westenberg JJ. CMR for assessment of diastolic function. Curr Cardiovasc Imaging Rep 2011;4(2):149–58.
[4] Nagueh SF, Smiseth OA, Appleton CP, et al. Recommendations for the evaluation of left ventricular diastolic function by echocardiography: an update from the American Society of Echocardiography and the European Association of Cardiovascular Imaging. J Am Soc Echocardiogr 2016;29(4):277–314.
[5] Paelinck BP, de Roos A, Bax JJ, et al. Feasibility of tissue magnetic resonance imaging: a pilot study in comparison with tissue Doppler imaging and invasive measurement. J Am Coll Cardiol 2005;45(7):1109–16.
[6] Rathi VK, Doyle M, Yamrozik J, et al. Routine evaluation of left ventricular diastolic function by cardiovascular magnetic resonance: a practical approach. J Cardiovasc Magn Reson 2008;10:36.
[7] Moreo A, Ambrosio G, De Chiara B, et al. Influence of myocardial fibrosis on left ventricular diastolic function: noninvasive assessment by cardiac magnetic resonance and echo. Circ Cardiovasc Imaging 2009;2(6):437–43.
[8] Moreo A, Ambrosio G, De Chiara B, Tran T, Raman SV. Influence of midwall fibrosis on diastolic dysfunction in non-ischemic cardiomyopathy. J Cardiovasc Magn Reson 2009;11:56. (20042111).
[9] Giri S, Chung YC, Merchant A, et al. T2 quantification for improved detection of myocardial edema. J Cardiovasc Magn Reson 2009;11:56.
[10] Thavendiranathan P, Walls M, Giri S, et al. Improved detection of myocardial involvement in acute inflammatory cardiomyopathies using T2 mapping. Circ Cardiovasc Imaging 2012;5(1):102–10.
[11] Verhaert D, Thavendiranathan P, Giri S, et al. Direct T2 quantification of myocardial edema in acute ischemic injury. JACC Cardiovasc Imaging 2011;4(3):269–78.
[12] Ommen SR, Nishimura RA, Appleton CP, et al. Clinical utility of Doppler echocardiography and tissue Doppler imaging in the estimation of left ventricular filling pressures: a comparative simultaneous Doppler-catheterization study. Circulation 2000;102(15):1788–94.
[13] Andre F, Steen H, Matheis P, et al. Age- and gender-related normal left ventricular deformation assessed by cardiovascular magnetic resonance feature tracking. J Cardiovasc Magn Reson 2015;17:25.
[14] Sohn DW, Chai IH, Lee DJ, et al. Assessment of mitral annulus velocity by Doppler tissue imaging in the evaluation of left ventricular diastolic function. J Am Coll Cardiol 1997;30(2):474–80.
[15] Ha JW, Ommen SR, Tajik AJ, et al. Differentiation of constrictive pericarditis from restrictive cardiomyopathy using mitral annular velocity by tissue Doppler echocardiography. Am J Cardiol 2004;94(3):316–9.
[16] Rajagopalan N, Garcia MJ, Rodriguez L, et al. Comparison of new Doppler echocardiographic methods to differentiate constrictive pericardial heart disease and restrictive cardiomyopathy. Am J Cardiol 2001;87(1):86–94.
[17] Bollache E, Redheuil A, Clement-Guinaudeau S, et al. Automated left ventricular diastolic function evaluation from phase-contrast cardiovascular magnetic resonance and comparison with Doppler echocardiography. J Cardiovasc Magn Reson 2010;12:63.
[18] Gatehouse PD, Rolf MP, Graves MJ, et al. Flow measurement by cardiovascular magnetic resonance: a multi-centre multi-vendor study of background phase offset errors that can compromise the accuracy of derived regurgitant or shunt flow measurements. J Cardiovasc Magn Reson 2010;12:5.
[19] Kilner PJ, Gatehouse PD, Firmin DN. Flow measurement by magnetic resonance: a unique asset worth optimising. J Cardiovasc Magn Reson 2007;9(4):723–8.
[20] Morton G, Schuster A, Jogiya R, Kutty S, Beerbaum P, Nagel E. Inter-study reproducibility of cardiovascular magnetic resonance myocardial feature tracking. J Cardiovasc Magn Reson 2012;14:43.
[21] Augustine D, Lewandowski AJ, Lazdam M, et al. Global and regional left ventricular myocardial deformation measures by magnetic resonance feature tracking in healthy volunteers: comparison with tagging and relevance of gender. J Cardiovasc Magn Reson 2013;15:8.
[22] Weale P, Guetter C, Collins J, et al. A novel, automated method for measuring mitral valve annular velocity from standard cine TruFISP data - a feasibility study. J Cardiovasc Magn Reson 2011;13(Suppl. 1):O48.
[23] Saba SG, Chung S, Bhagavatula S, et al. A novel and practical cardiovascular magnetic resonance method to quantify mitral annular excursion and recoil applied to hypertrophic cardiomyopathy. J Cardiovasc Magn Reson 2014;16:35.

[24] Wu V, Chyou JY, Chung S, Bhagavatula S, Axel L. Evaluation of diastolic function by three-dimensional volume tracking of the mitral annulus with cardiovascular magnetic resonance: comparison with tissue Doppler imaging. J Cardiovasc Magn Reson 2014;16:71.
[25] Guetter C, Chefd'hotel C, Xue H, G J. Efficient symmetric and inverse-consistent deformable registration. Proceedings ISBI. 2011. p. 590–3.
[26] Lu X, Georgescu B, Jolly MP, et al. Cardiac anchoring in MRI through context modeling. Med Image Comput Comput Assist Interv 2010;13(Pt 1):383–90.
[27] Georgescu B, Zhou X, Comaniciu D, Gupta A. Database-guided segmentation of anatomical structures with complex apperance. Proceedings IEEE. 2. 2005.
[28] Viola P, Jones MJ. Robust real-time face detection. Int J Comput Vis 2004;57(2):137–54.
[29] Hoaglin DC, Inglewicz B. Fine tuning some resistant rules for outlier labeling. J Am Stat Assoc 1987;82:1147–9.
[30] Nagueh SF, Appleton CP, Gillebert TC, et al. Recommendations for the evaluation of left ventricular diastolic function by echocardiography. J Am Soc Echocardiogr 2009;22(2):107–33.
[31] Go AS, Mozaffarian D, Roger VL, et al. Heart disease and stroke statistics—2013 update a report from the American Heart Association. Circulation. 2012.
[32] Chen HH, Lainchbury JG, Senni M, Bailey KR, Redfield MM. Diastolic heart failure in the community: clinical profile, natural history, therapy, and impact of proposed diagnostic criteria. J Card Fail 2002;8(5):279–87.
[33] McCullough PA, Khandelwal AK, McKinnon JE, et al. Outcomes and prognostic factors of systolic as compared with diastolic heart failure in urban America. Congest Heart Fail 2005;11(1):6–11.
[34] Hillis GS, Moller JE, Pellikka PA, et al. Noninvasive estimation of left ventricular filling pressure by E/e′ is a powerful predictor of survival after acute myocardial infarction. J Am Coll Cardiol 2004;43(3):360–7.
[35] Buss SJ, Krautz B, Schnackenburg B, et al. Classification of diastolic function with phase-contrast cardiac magnetic resonance imaging: validation with echocardiography and age-related reference values. Clin Res Cardiol 2014;103(6):441–50.
[36] Marsan NA, Westenberg JJ, Tops LF, et al. Comparison between tissue Doppler imaging and velocity-encoded magnetic resonance imaging for measurement of myocardial velocities, assessment of left ventricular dyssynchrony, and estimation of left ventricular filling pressures in patients with ischemic cardiomyopathy. Am J Cardiol 2008;102(10):1366–72.
[37] Schuster A, Hor KN, Kowallick JT, Beerbaum P, Kutty S. Cardiovascular magnetic resonance myocardial feature tracking: concepts and clinical applications. Circ Cardiovasc Imaging 2016;9(4):e004077.
[38] Kowallick JT, Kutty S, Edelmann F, et al. Quantification of left atrial strain and strain rate using cardiovascular magnetic resonance myocardial feature tracking: a feasibility study. J Cardiovasc Magn Reson 2014;16:60.
[39] von Roeder M, Rommel KP, Kowallick JT, et al. Influence of left atrial function on exercise capacity and left ventricular function in patients with heart failure and preserved ejection fraction. Circ Cardiovasc Imaging 2017;10(4).